IEEE Access
Multidisciplinary ⋮ Rapid Review ⋮ Open Access Journal

Received 16 April 2024, accepted 27 May 2024, date of publication 3 June 2024, date of current version 10 June 2024.

Digital Object Identifier 10.1109/ACCESS.2024.3408288

RESEARCH ARTICLE

Transmit Diversity-Achieving Quadrature Index Modulation Aided Media-Based Modulation

XIAOPIN WANG[1], SHUQING LIN[2], AND FUCHUN HUANG[1,2]
[1]Software Engineering Institute of Guangzhou, Guangzhou 510990, China
[2]Guangzhou College of Commerce, Guangzhou 511363, China

Corresponding author: Shuqing Lin (20061018@gcc.edu.cn)

This work was supported by the Basic and Applied Basic Research Project, Guangzhou Basic Research Plan under Grant 202201011680.

ABSTRACT In this paper, a new schematic of quadrature index modulation (QIM) with generalized spatial constellations is proposed and amalgamated with the media-based modulation (MBM) system for not only achieving the transmit diversity gains but also increasing the spectral efficiency (SE). Based on this, this new scheme may be named as Transmit Diversity-achieving QIM-MBM (TD-QIM-MBM). Specifically, all available transmit antennas (TAs), whose each TA is equipped with n_{rf} radio frequency (RF) mirrors, are firstly grouped into G groups of TAs, each group of which is assigned to one corresponding Bits-Modulator. Then, one mapped three dimension (3D) signal constellation point (CP) is copied into G versions and then are respectively fed into G groups of Bits-Modulators. In each group of Bits-Modulator, with the aid of the antenna index (AI) bits of three spatial domains, one version of 3D signal CP is modulated into one QIM vector symbol. Furthermore, the in-phase and quadrature vectors of the QIM vector symbol are respectively modulated on the specified channel states with the in-phase and quadrature channel index (CI) bits and then formed into one MBM vector symbol. On the design of G groups of Bits-Modulators, G MBM vector symbols are obtained and concatenated into one transmitted MBM vector (TMV) symbol. Finally, in order to outstand the advantage of the proposed TD-QIM-MBM, the SEs and the squared minimum Euclidean distances (MEDs) of the TD-QIM-MBM are provided in comparisons with other schemes, and the average bit error probability is also provided. In simulation results with the Monte Carlo method, it demonstrates that the TD-QIM-MBM outperforms the classic design schemes (e.g., GSM-MBM and QSM-MBM) in terms of the bit error rate (BER) performance for enhancing the reliability of MBM-based wireless communications.

INDEX TERMS Quadrature index modulation (QIM), media-based modulation (MBM), transmit diversity, bits-modulator, minimum Euclidean distances (MEDs).

I. INTRODUCTION

In the multiple-input multiple-output with index modulation (MIMO-IM) systems, utilizing the IM technique to exploit the additional information with the exploitation of the index domains such as the indexes of spatial index domain [1], [2], [3], [4], [5], [6], not only the spectral efficiency (SE) but also the reliability of the communication systems have been effectively enhanced. In the generalized spatial modulation (GSM) [1], the multiplex gain is effectively achieved by making full use of the idle transmit antennas (TAs) in the spatial domain. In the quadrature SM (QSM) system [2], the spatial domain is extended to the in-phase and quadrature dimensions for modulating the real and imaginary parts of the modulated symbol from the QAM/PSK constellation, respectively. Then, to enhance the SE, a transmit vector [3] is obtained by a fold vector with multiple QSM symbols. In [4], utilizing the spatial domain of TAs, the generalized QSM is proposed to improve the SE with the grouping of available TAs. In order to extend the spatial domain without considering the antenna grouping, utilizing the characteristic of the squared minimum Euclidean distance (MED) between the transmit vectors, two different signal constellations (conventional QAM and secondary QAM) are combined to further develop the spatial index domain [5]. Such that more antenna index (AI) information is exploited.

The associate editor coordinating the review of this manuscript and approving it for publication was Yafei Hou.

In addition, signed QSM (SQSM) [6] is further proposed to double the spatial domain of the QSM. However, double the AI information is achieved at the cost of decreasing the number of signal constellation points (CPs) in the QAM constellation.

In view of the limitation of the spatial dimension, except that carrying additional information in the spatial domain, multiple index domains [7], [8], [9] have also been developed. By the expanding of both the TA space and signal CP domains, quadrature index modulation (QIM) [7] is proposed to enhance the reliability of wireless communications. In the QIM, which differs from the QSM, the spatial domain of the TAs is developed into three dimensionality and then to be respectively used to convey three components of the mapped three dimension (3D) signal CP for enhancing the transmission of the additional information, i.e., The in-phase spatial domain of the TAs is developed into two dimensionality for respectively modulating two components of the mapped 3D signal CP, and the quadrature spatial domain of the TAs is designed to modulate the remain component of the mapped 3D signal CP. In [8], utilizing the difference of two signal constellations, the GSM with multi-index modulation (GSM-MIM) is proposed to develop two types of both the switch index and vector index for not only carrying the additional information but also increasing the squared MED between the transmit vectors. Furthermore, In the spatial modulation with spatial constellation (SM-SC) [9], the group index (GI) domain is developed. In order to enhance the SE by further exploiting other index domains, the permutation technique [10] and Walsh-Hadamard code [11], [12] are investigated. In [10], on basis of the framework of the SM-SC technique, the spatial modulation with jointing permutation, group and antenna indexes (JPGA-ISM) is proposed to design the permutation index (PI) matrix with two algorithms. In addition, Walsh-Hadamard code [11], [12] is provided for the code index information.

To some extent, the additional information carried by the index domains has been increased based on the above-mentioned works in the MIMO-IM systems. However, the space domain of TAs has not been significantly expanded for combating channel fading. In terms of the channel states, media based modulation (MBM) [13], the concept of which is proposed to embed information to the variables of channel states, achieves the significant gains of performance over traditional single-input multiple-output (SIMO) systems by designing radio frequency (RF) mirrors. In order to expand the spatial freedom of the TAs at the transmitter, inspired by the space shift key (SSK) [14], the channel modulation (CM) technique with the channel state domain is developed to carry the channel index (CI) information when each TA is equipped with multiple mirrors. Subsequently, to achieve a high SE and improve the bit error rate (BER) performance in the SIMO systems, the MBM technique aided the SIMO (SIMO-MBM) systems are proposed in [15], [16], and [17]. In the MAP-index coded MBM (MIC-MBM) [15], Reed-Solomon encoder encodes the MAP-index into the elements in a Galois field across time. Such that the MIC-MBM has good distance distribution for improving the BER performance as compared with the traditional MBM system. Furthermore, the optimum irregular hexagonal QAM aided the MBM system [16] is designed to achieve not only the higher SE and but also energy-efficient compared with the traditional MBM with the QAM constellation. Utilizing the quadrature dimension of spatial constellation, QSM aided SIMO-MBM [17] is proposed to further enhance the SE with the CI information in the in-phase and quadrature dimensions.

For greatly increasing the SE and the reliability of wireless communications, a lot of works on integrating the MIMO-IM systems into the CM system are investigated in [18], [19], and [20]. In other words, the additional information is composed of both the spatial index information and the CI information. In [18], the SM-, GSM-MBM are designed by jointing developing the spatial index domain and the CI domain, e.g., In the GSM-MBM, each TA is equipped with a MBM-unit having n_{rf} mirrors that generates $2^{n_{\mathrm{rf}}}$ mirror activation patterns (MAPs) for the selection of the CI bits, Thus, with n_{a} active TAs, the total number of additional information conveyed has $n_{\mathrm{a}} \cdot \lfloor \log_2(\binom{N_{\mathrm{t}}}{n_{\mathrm{a}}}) \rfloor + n_{\mathrm{a}} \cdot n_{\mathrm{rf}}$ bits, where N_{t} is the number of total TAs and active TAs. In [19], the QSM is directly applied to the MBM system with the consideration of two cases: the same and different active TAs for the real and imaginary parts of the modulated symbol. With the design of one reserved TA, quadrature channel modulation-III (QCM-III) [20] is proposed to not only retain the merit of the QSM but also convey the CI information in the in-phase and quadrature dimensions, i.e., $2\log_2 N_{\mathrm{t}} + 2n_{\mathrm{rf}}$ bits.

Although the SE and the reliability of transmission link have been improved, the transmit diversity has not been well investigated on the above-mentioned research works. In recent years, to achieve the transmit diversity, the time domain is considered to be extended. In [21] and [22], the concept of space-time block code (STBC) [23] is applied to the MBM system. In both space-time channel modulation (STCM) [21] and space-time MBM [22], the diversity gains are achieved by combining the CM with the STBC in two time-slots. Furthermore, utilizing the selected dispersion matrixes, the QSM-MBM [24] modulates the in-phase/quadrature part of one QSM symbol with half of the available TAs into a QSM matrix vector. Thus, the QSM-MBM not only achieves the TD but also is capable of improving the SE with multiple indexes of the TAs, channel states and DMs. However, the transmit diversity is achieved at the cost of the time slots. During each time-slot, this work [25], called as single-symbol GSM-MBM (S-GSM-MBM), achieves the transmit diversity through one modulated symbol is transmitted on multiple channel states corresponding to multiple active TAs, respectively. Although the transmit diversity gain is obtained, the number of transmitted spatial index information bits is only

$\lfloor \log_2(\binom{N_t}{n_a}) \rfloor$, which is determined by the combinations of active TAs.

Considering the previous works, in order to further enhance the SE by utilizing multiple index domains and the reliability of wireless communications by achieving the transmit diversity, the transmit diversity-achieving quadrature index modulation aided MBM (TD-QIM-MBM) is investigated by utilizing three space dimensionality of the TAs in the QIM and the antenna grouping technique. Our contributions of this paper are as below:

1) On basis of integrating the design idea of the QIM into the MBM system, the framework of the TD-QIM-MBM system is developed. Specifically, all available TAs are firstly grouped into G groups for G modules of Bits-Modulators, each TA in each group is equipped with one MBM-Unit having $n_{\rm rf}$ mirrors. Then, each module of Bits-Modulator is used to modulate each bits-block of $B_g, g \in \{1, \cdots, G\}$ and one and the same 3D mapped symbol $s_{\rm 3D}(m_x, m_y, m_z)$ into one spatial MBM vector symbol to be transmitted over the specified channel states with the in-phase and quadrature CI information.
2) On the one hand, aiming at achieving the transmit diversity, each module of Bits-Modulator is used to modulate one of G versions obtained by coping the mapped 3D signal CP. On the other hand, to improve the higher SE, three AI vectors are respectively designed to modulate three components of the input 3D mapped symbol, resulting in the in-phase and quadrature spatial vector (SV) symbols: the in-phase SV $\mathbf{S}$ and $\mathbf{C}$, i.e., three components m_x, m_y, m_z are modulated on the specified TAs with the AI information. Then, with the aid of the in-phase and quadrature CI bits, the in-phase SV $\mathbf{S}$ and $\mathbf{C}$ are transmitted over the specified channel states, i.e., forming one spatial transmitted MBM vector (TMV) symbol.
3) The squared MEDs between the TMVs are analyzed to outstand the advantage of the TD-QIM-MBM as compared with the classic MBM with index modulation (MBM-IM) at the different SEs. Furthermore, the average bit error probability (BEP) is analyzed with the employment of the Maximum Likelihood (ML) detector at the receiver. In our simulation results with the Monte Carlo method, compared with the GSM-MBM and QCM-III systems, the TD-QIM-MBM system is demonstrated that not only the BER performance but also the SE are enhanced in wireless communications.

The organization of this paper is as below. System model of TD-QIM-MBM is introduced in Section II. The performance analysis is provided in Section III. Section IV presents the comparisons of simulation results for different schemes. In Section V, we gives our conclusions.

TABLE 1. Examples of the mapping relations between the CI bits of $n_{\rm rf} = 3$ and 2^3 possible MAPs for the corresponding channel states.

$I_{\rm rf}^{g,\Re}/I_{\rm rf}^{g,\Im}$	$n_{\rm rf} = 3$ and 2^3 possible MAPs at $n_{\rm t}$-th TA		
	RF Mirror 1, 2, 3	MAP Index	Corresponding Channel State
0 0 0	OFF, OFF, OFF	1	$\mathbf{h}_1^{n_{\rm t}}$
0 0 1	OFF, OFF, ON	2	$\mathbf{h}_2^{n_{\rm t}}$
0 1 0	OFF, ON, OFF	3	$\mathbf{h}_3^{n_{\rm t}}$
0 1 1	OFF, ON, ON	4	$\mathbf{h}_4^{n_{\rm t}}$
1 0 0	ON, OFF, OFF	5	$\mathbf{h}_5^{n_{\rm t}}$
1 0 1	ON, OFF, ON	6	$\mathbf{h}_6^{n_{\rm t}}$
1 1 0	ON, ON, OFF	7	$\mathbf{h}_7^{n_{\rm t}}$
1 1 1	ON, ON, ON	8	$\mathbf{h}_8^{n_{\rm t}}$

II. THE PROPOSED TD-QIM-MBM

In this section, as shown in Fig. 1, we introduce the new schematic of the TD-QIM-MBM system having $N_{\rm t}$ TAs and $N_{\rm r}$ receive antennas, which is mainly composed of G modules of Bits-Modulator and $N_{\rm t}$ MBM-Units at the transmitter. Furthermore, the g-th Bits-Modulator module is equipped with $N_g, g \in \{1, \cdots, G\}$ TAs and each TA is arranged one MBM-Unit that is surrounded by $n_{\rm rf}$ RF mirrors (i.e., Corresponding to $n_{\rm rf}$ CI bits in each spatial dimension), where $n_{\rm rf}$ RF mirrors in each MBM-Unit can form $N_{\rm rf} = 2^{n_{\rm rf}}$ possible MAPs, as shown in TABLE 1: the mapping relations between the CI bits of $n_{\rm rf} = 3$ and 2^3 possible MAPs for the channel states: $[\mathbf{h}_1^{n_{\rm t}}, \cdots, \mathbf{h}_8^{n_{\rm t}}]$ that are introduced in (2) at the $n_{\rm t}$-th TA ($1 \le n_{\rm t} \le N_{\rm t}$). In TABLE 1, $I_{\rm rf}^{g,\Re}$ and $I_{\rm rf}^{g,\Im}$ are the CI information bits in the in-phase and quadrature dimensions, respectively. Note that, in Fig. 1 these parameters of $N_1, N_2, \cdots, N_G$ may be equal to or not, and $N_{\rm t} = N_1 + N_2 + \cdots + N_G$, N_g is an even number.

As is depicted in Fig. 1, with the signal CP $s_{\rm 3D}$ mapped by the bit block of $B_{\rm 3D}$, G modules of Bits-Modulator are used to modulate G groups of bits block: $B_1, \cdots, B_G$ into one spatial TMV $\mathbf{Z}$ with the size of $N_{\rm t}N_{\rm rf} \times 1$, which will be introduced in the following subsection. In the following, we introduce the system model of the TD-QIM-MBM and the design of spatial MBM vectors in detail.

A. SYSTEM MODEL

In the system model of the proposed TD-QIM-MBM depicted in Fig 1, the incoming bits sequence B are fed into the input of the TD-QIM-MBM and then split into $G + 1$ groups of bits block: $B_1, \cdots, B_G$ and $B_{\rm 3D}$ through the block of Bits Stream Splitter for Multi-Groups. Then, the block of $B_{\rm 3D}$ is fed into the 3D Signal Mapper and mapped into a 3D signal CP $s_{\rm 3D}$ from the 3D signal constellation reported in [7]. Subsequently, the mapped 3D signal CP $s_{\rm 3D}$ is copied into G versions and then fed into G Modules of Bits-Modulator. Furthermore, utilizing G Modules of Bits-Modulator, G groups of bits block: $B_1, \cdot, B_G$ are used to modulate one same mapped 3D signal symbol $s_{\rm 3D}$ into G spatial MBM vectors: $\mathbf{Z}^1 \in C^{1\times N_1 \cdot N_{\rm rf}}, \mathbf{Z}^2 \in C^{1\times N_2 \cdot N_{\rm rf}}, \cdots, \mathbf{Z}^G \in C^{1\times N_G \cdot N_{\rm rf}}$, whose g-th spatial MBM vector consists of N_g number of $\mathbf{X}_1^g \in C^{1\times N_{\rm rf}}, \mathbf{X}_2^g \in C^{1\times N_{\rm rf}}, \cdots, \mathbf{X}_{N_g}^g \in C^{1\times N_{\rm rf}}$, which will be detailedly introduced in Section II-B. That is to say, the

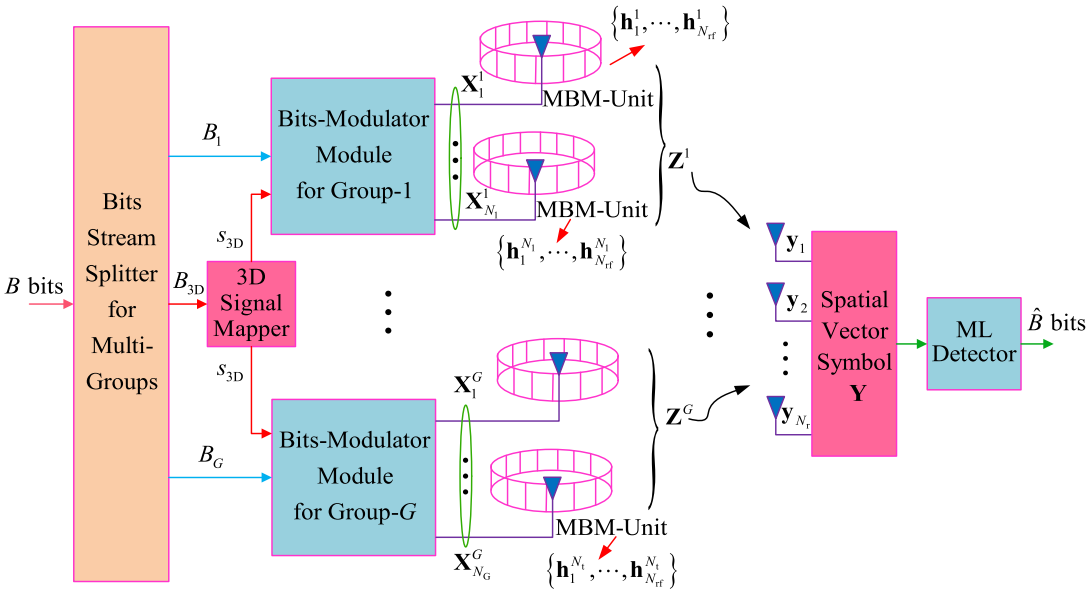

FIGURE 1. System model of the TD-QIM-MBM.

normalized spatial TMV symbol can be expressed by

$$\bar{\mathbf{Z}} = \frac{1}{G} \cdot [\mathbf{Z}^1, \mathbf{Z}^2, \cdots, \mathbf{Z}^G]^T \tag{1}$$

where the sign of $[\cdot]^T$ denotes the operation of the transposition. In addition, with N_{t} number of TAs, each with n_{rf} RF mirrors, as previously described, it has $N_{\mathrm{rf}} = 2^{n_{\mathrm{rf}}}$ MAPs corresponding to $2^{n_{\mathrm{rf}}}$ channel states expressed by $\mathbf{H}_{n_{\mathrm{t}}} = [\mathbf{h}_1^{n_{\mathrm{t}}}, \cdots, \mathbf{h}_{N_{\mathrm{rf}}}^{n_{\mathrm{t}}}]$ at the n_{t}-th TA. Hence, the channel matrix $\mathbf{H}$ with N_{t} TAs can be expressed as

$$\begin{aligned}\mathbf{H} &= [\mathbf{H}_1, \mathbf{H}_2, \cdots, \mathbf{H}_{N_{\mathrm{t}}}] \\ &= [\underbrace{\mathbf{h}_1^1, \cdots, \mathbf{h}_{N_{\mathrm{rf}}}^1}_{1-\text{st TA}}, \underbrace{\mathbf{h}_1^2, \cdots, \mathbf{h}_{N_{\mathrm{rf}}}^2}_{2-\text{nd TA}}, \cdots, \underbrace{\mathbf{h}_1^{N_{\mathrm{t}}}, \cdots, \mathbf{h}_{N_{\mathrm{rf}}}^{N_{\mathrm{t}}}}_{N_{\mathrm{t}}-\text{th TA}}],\end{aligned} \tag{2}$$

where $\mathbf{H} \in C^{N_{\mathrm{r}} \times N_{\mathrm{t}} N_{\mathrm{rf}}}$, $\mathbf{h}_\lambda^{n_{\mathrm{t}}} \in C^{N_{\mathrm{r}} \times 1}$, $\lambda \in \{1, \cdots, N_{\mathrm{rf}}\}$ obeys the Rayleigh fading with each element following $CN(0, 1)$, the additive white Gaussian noise vector $\mathbf{N} \in C^{N_{\mathrm{r}} \times 1}$ follows zero-mean and variance σ^2, i.e., $CN(0, \sigma^2)$.

After that the spatial TMV symbol $\bar{\mathbf{Z}}$ with G versions of the mapped 3D symbol $s_{3\mathrm{D}}$ is transmitted over the selected channel states from the channel matrix $\mathbf{H}$ with the CI bits of both $I_{\mathrm{rf}}^{g,\Re}$ and $I_{\mathrm{rf}}^{g,\Im}$. Thus, the receiver signal vector for the TD-QIM-MBM system can be expressed as (3), as shown at the bottom of the next page, where $\mathbf{Y} \in C^{N_{\mathrm{r}} \times 1}$, $\varsigma_g = N_1 + \cdots + N_g$.

B. DESIGN OF SPATIAL MBM VECTORS

In the following subsection, the design of each Bits-Modulator is introduced. Since each Bits-Modulator has the same the design method, without loss of generality, we only introduce the design principle of one of G Bits-Modulators in this subsection. For the g-th Bits-Modulator, N_g MBM vectors $\mathbf{X}_1^g, \cdots, \mathbf{X}_{N_g}^g$ with the size of $N_g \times 1$ dimension are generated in the g-th module of Bits-Modulator.

As is described in Fig. 2, the mapped 3D symbol $s_{3\mathrm{D}}$ is decomposed by the Component Decomposer into three components: m_x, m_y, m_z after being fed into the g-th Bits-Modulator. Furthermore, the bits block of B_g is fed into the g-th module of Bits-Modulator and then split into five subblocks: $I_{\mathrm{rf}}^{g,\Re}$ and $I_{\mathrm{rf}}^{g,\Im}$ for the CI information bits in the in-phase and quadrature dimensions, $I_{\bar{\mathrm{A}}}^g$, $I_{\bar{\mathrm{B}}}^g$ and $I_{\bar{\mathrm{C}}}^g$ for the antenna index (AI) bits of three spatial domains.

Specifically, in the AI Vector Selector $\bar{\mathrm{A}}$, the subblock of $I_{\bar{\mathrm{A}}}^g$ is employed to select an AI vector $\mathbf{a}_{i^g}$ from the AI vector set $\Omega_{\bar{\mathrm{A}}} = \left\{\mathbf{a}_1, \mathbf{a}_2, \cdots, \mathbf{a}_{N_{\mathrm{g}}/2}\right\}$, where i^g is obtained by adding 1 to the decimal representation of the bit subblock $I_{\bar{\mathrm{A}}}^g$. Similarly, in the AI Vector Selector $\bar{\mathrm{B}}$, the subblock of $I_{\bar{\mathrm{B}}}^g$ is used to select an AI vector $\mathbf{b}_{\ell^g}$ from the AI vector set $\Omega_{\bar{\mathrm{B}}} = \left\{\mathbf{b}_1, \mathbf{b}_2, \cdots, \mathbf{b}_{N_{\mathrm{g}}/2}\right\}$, where ℓ^g is obtained by adding 1 to the decimal representation of the bit subblock $I_{\bar{\mathrm{B}}}^g$. Note that, when simultaneously modulating two components m_x, m_y of the mapped 3D symbol $s_{3\mathrm{D}}$ by two selected AI vectors $\mathbf{a}_{i^g}$, $\mathbf{b}_{\ell^g}$, the overlap between two components m_x, m_y should not be allowed to occur. Thus, the design for two sets of both $\Omega_{\bar{\mathrm{A}}}$ and $\Omega_{\bar{\mathrm{B}}}$ are further introduced in the following. For the set of $\Omega_{\bar{\mathrm{A}}}$, $\frac{N_{\mathrm{g}}}{2}$ number of AI vectors: $\mathbf{a}_1, \mathbf{a}_2, \cdots, \mathbf{a}_{N_{\mathrm{g}}/2}$ respectively correspond to $\frac{N_{\mathrm{g}}}{2}$ column vectors of the matrix $\mathbf{A}$ with $N_{\mathrm{g}} \times \frac{N_{\mathrm{g}}}{2}$ dimensions, which can be expressed by

$$\mathbf{A} = \begin{bmatrix} \mathbf{I}_{\frac{N_{\mathrm{g}}}{2} \times \frac{N_{\mathrm{g}}}{2}} \\ \mathbf{0}_{\frac{N_{\mathrm{g}}}{2} \times \frac{N_{\mathrm{g}}}{2}} \end{bmatrix}, \tag{4}$$

where $\mathbf{I}_{\frac{N_{\mathrm{g}}}{2} \times \frac{N_{\mathrm{g}}}{2}}$ is an unit matrix with the size of $\frac{N_{\mathrm{g}}}{2} \times \frac{N_{\mathrm{g}}}{2}$, $\mathbf{0}_{\frac{N_{\mathrm{g}}}{2} \times \frac{N_{\mathrm{g}}}{2}}$ is a zero matrix with the size of $\frac{N_{\mathrm{g}}}{2} \times \frac{N_{\mathrm{g}}}{2}$. Similarly, the set of $\Omega_{\bar{\mathrm{B}}}$ can be designed. However, in order to avoid the overlap between two components of both m_x

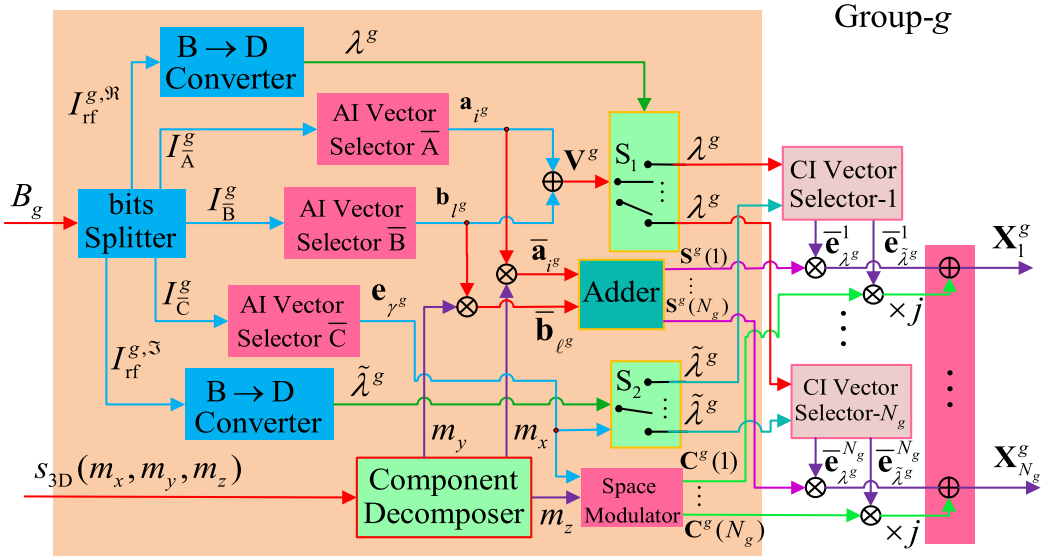

FIGURE 2. Design of the g-th group of Bits-Modulator.

and m_y, the $N_g \times \frac{N_g}{2}$ dimensional matrix $\mathbf{B}$ having the corresponding $\frac{N_g}{2}$ column vectors for $\frac{N_g}{2}$ number of AI vectors: $\mathbf{b}_1, \mathbf{b}_2, \cdots, \mathbf{b}_{N_g/2}$ can be expressed by

$$\mathbf{B} = \begin{bmatrix} \mathbf{0}_{\frac{N_g}{2} \times \frac{N_g}{2}} \\ \mathbf{I}_{\frac{N_g}{2} \times \frac{N_g}{2}} \end{bmatrix}. \tag{5}$$

Based on the above design, we can obtain the number of AI information bits for both $I_{\bar{\mathrm{A}}}^g$ and $I_{\bar{\mathrm{B}}}^g$, which are expressed as $I_{\bar{\mathrm{A}}}^g = \left\lfloor \log_2 \frac{N_g}{2} \right\rfloor$ and $I_{\bar{\mathrm{B}}}^g = \left\lfloor \log_2 \frac{N_g}{2} \right\rfloor$, respectively.

Then, two selected AI vectors $\mathbf{a}_{i^g}, \mathbf{b}_{\ell^g}$ respectively modulate two components m_x, m_y with the aid of two multipliers, resulting in two spatial vectors: $\bar{\mathbf{a}}_{i^g} = m_x \cdot \mathbf{a}_{i^g}, \bar{\mathbf{b}}_{\ell^g} = m_y \cdot \mathbf{b}_{\ell^g}$. Finally, performing the operation of the Adder, the $N_g \times 1$ dimensional spatial vector symbol $\mathbf{S}^g$ is obtained and can be expressed as

$$\mathbf{S}^g = \begin{bmatrix} \mathbf{S}^g(1) \\ \mathbf{S}^g(2) \\ \vdots \\ \mathbf{S}^g(N_g) \end{bmatrix}$$

$$= \bar{\mathbf{a}}_{i^g} + \bar{\mathbf{b}}_{\ell^g} = m_x \cdot \mathbf{a}_{i^g} + m_y \cdot \mathbf{b}_{\ell^g}. \tag{6}$$

where $\mathbf{S}^g(1), \mathbf{S}^g(2) \ldots \mathbf{S}^g(N_g) \in \{0, m_x, m_y\}$. Note that $\mathbf{S}^g(i^g) = m_x, \mathbf{S}^g(\frac{N_g}{2} + \ell^g) = m_y$.

For the two subblocks of both $I_{\mathrm{rf}}^{g,\Re}$ and $I_{\mathrm{rf}}^{g,\Im}$, using the B→D Converters to convert them into the decimal numbers: λ^g, $\tilde{\lambda}^g$. On the one hand, the spatial vector $\mathbf{V}^g$ used to control two Switches of the $2 \times N_g$ Switch Controller S_1 are obtained by adding the $\mathbf{a}_{i^g}$ and $\mathbf{a}_{\ell^g}$, which can be expressed by

$$\mathbf{V}^g = [\overbrace{0 \cdots \underbrace{1}_{i^g} \cdots 0}^{\frac{N_g}{2}\text{components}} \overbrace{0 \cdots \underbrace{1}_{(\frac{N_g}{2}+\ell^g)} \cdots 0}^{\frac{N_g}{2}\text{components}}]^T. \tag{7}$$

Furthermore, according to the row index numbers from two non-zero elements in the spatial vector $\mathbf{V}^g$, the $2 \times N_g$ Switch Controller S_1 feeds the CI number λ^g into the i^g, $(\frac{N_g}{2} + \ell^g)$-th CI Vector Selectors, i.e., the two CI Vector Selector-i^g, -$(\frac{N_g}{2} + \ell^g)$.

Then, with the CI number λ^g, the λ^g-th CI $\mathbf{e}_{\lambda^g}^{i^g}$ is selected from the CI vector set $\Delta^{i^g} = \left\{\bar{\mathbf{e}}_1^{i^g}, \cdots, \bar{\mathbf{e}}_{N_{\mathrm{rf}}}^{i^g}\right\}$ whose N_{rf}

$$\begin{aligned}
\mathbf{Y} &= \mathbf{H} \cdot \bar{\mathbf{Z}} + \mathbf{N} \\
&= [\mathbf{H}_1, \mathbf{H}_2, \cdots, \mathbf{H}_{N_t}] \cdot \frac{1}{G} \left[\mathbf{Z}^1, \mathbf{Z}^2, \cdots, \mathbf{Z}^G\right]^T + \mathbf{N} \\
&= [\mathbf{H}_1, \mathbf{H}_2, \cdots, \mathbf{H}_{N_t}] \cdot \frac{1}{G} \left[\underbrace{\mathbf{X}_1^1, \cdots, \mathbf{X}_{N_1}^1}_{1-\text{st Group}}, \underbrace{\mathbf{X}_1^2, \cdots, \mathbf{X}_{N_2}^2}_{2-\text{nd Group}}, \cdots, \underbrace{\mathbf{X}_1^G, \cdots, \mathbf{X}_{N_G}^G}_{G-\text{th Group}}\right]^T + \mathbf{N} \\
&= \frac{1}{G} \cdot \{\underbrace{\mathbf{H}_1(\mathbf{X}_1^1)^T + \cdots, \mathbf{H}_{N_1}(\mathbf{X}_{N_1}^1)^T}_{1-\text{st Group}} + \underbrace{\mathbf{H}_{N_1+1}(\mathbf{X}_1^2)^T + \cdots + \mathbf{H}_{\varsigma_2}(\mathbf{X}_{N_2}^2)^T}_{2-\text{nd Group}} + \cdots + \underbrace{\mathbf{H}_{\varsigma_{G-1}+1}(\mathbf{X}_1^G)^T + \cdots + \mathbf{H}_{\varsigma_G}(\mathbf{X}_{N_G}^G)^T}_{G-\text{th Group}}\} + \mathbf{N}
\end{aligned} \tag{3}$$

CI vectors are used to specify the channel states (e.g., $\{\mathbf{h}_1^{i^g}, \mathbf{h}_2^{i^g}, \cdots, \mathbf{h}_{N_{\rm rf}}^{i^g}\}$) on the i^g active TA, where $\bar{\mathbf{e}}_{\lambda^g}^{i^g}$ denotes the $N_{\rm rf} \times 1$ unit vector with the λ^g-th row non-zero element equaling to "1" to be used to specify the λ^g-th channel state $\mathbf{h}_{\lambda^g}^{i^g}$ of the channel states set $\mathbf{H}^{i^g} = \{\mathbf{h}_1^{i^g}, \mathbf{h}_2^{i^g}, \cdots, \mathbf{h}_{N_{\rm rf}}^{i^g}\}$. Finally, the component $\mathbf{S}^g(i^g)$ (i.e., m_x) of the $\mathbf{S}^g$ in (6) is modulated by the selected CI vector $\bar{\mathbf{e}}_{\lambda^g}^{i^g}$ on the specified channel state $\mathbf{h}_{\lambda^g}^{i^g}$ to be transmitted. Thus, the in-phase part of the i^g-th MBM vector symbol $\mathbf{X}_{i^g}^{g}$ on the i^g-th active TA can be expressed mathematically by

$$\mathbf{X}_{i^g}^{g,\Re} = [\bar{\mathbf{e}}_{\lambda^g}^{i^g} \cdot \mathbf{S}^g(i^g)]^T. \tag{8}$$

Similar to the above-mentioned design principle, the in-phase part of the $(\frac{N_{\rm g}}{2} + \ell^g)$-th MBM vector symbol $\mathbf{X}_{\frac{N_{\rm g}}{2}+\ell^g}^{g,\Re}$ on the $(\frac{N_{\rm g}}{2} + \ell^g)$-th active TA can be expressed mathematically by

$$\mathbf{X}_{\frac{N_{\rm g}}{2}+\ell^g}^{g,\Re} = [\bar{\mathbf{e}}_{\lambda^g}^{(\frac{N_{\rm g}}{2}+\ell^g)} \cdot \mathbf{S}^g(\frac{N_{\rm g}}{2} + \ell^g)]^T. \tag{9}$$

It is very important to note that the MBM vectors on unactive TAs in the in-phase dimension are set to zero vectors with the size of $1 \times N_{\rm rf}$ dimensions.

Therefore, according to the above-mentioned design, the in-phase part of the MBM vector symbol $\mathbf{Z}^g$ for the output of the g-th block of Bits-Modulator can be expressed as

$$\begin{aligned}\mathbf{Z}^{g,\Re} &= [\mathbf{X}_1^{g,\Re}, \cdots, \mathbf{X}_{N_g}^{g,\Re}] \\ &= [\mathbf{0}_1, \cdots, \mathbf{X}_{i^g}^{g,\Re}, \cdots, \mathbf{0}_{\frac{N_{\rm g}}{2}}, \cdots, \mathbf{X}_{\frac{N_{\rm g}}{2}+\ell^g}^{g,\Re}, \cdots, \mathbf{0}_{N_g}]\end{aligned} \tag{10}$$

where all zero vectors are the size of $1 \times N_{\rm rf}$ dimensions.

On the other hand, the remaining subblock of $I_{\bar{\rm C}}^g$, containing $I_{\bar{\rm C}}^g = \lfloor \log_2 N_{\rm g} \rfloor$ information bits, is used to select an AI vector $\mathbf{e}_{\gamma^g}$ from the AI vector set $\Omega_{\bar{\rm C}} = \{\mathbf{e}_1, \mathbf{e}_2, \cdots, \mathbf{e}_{N_{\rm g}}\}$, where $\mathbf{e}_1, \mathbf{e}_2, \cdots, \mathbf{e}_{N_{\rm g}}$ respectively corresponds to $N_{\rm g}$ columns of vector in one unit matrix $\mathbf{e}^g$ with the size of $N_{\rm g} \times N_{\rm g}$ dimensions, γ^g is obtained by adding 1 to the decimal representation of the bit subblock $I_{\bar{\rm C}}^g$. Then, through the Space Modulator, the $N_g \times 1$ dimensional spatial vector symbol $\mathbf{C}^g$ is obtained as $\mathbf{C}^g = \left[\mathbf{C}^g(1)\ \mathbf{C}^g(2) \cdots \mathbf{C}^g(N_g)\right]^T = m_z \cdot \mathbf{e}_{\gamma^g}$ by modulating the component m_z with the selected AI vector $\mathbf{e}_{\gamma^g}$, where $\mathbf{C}^g(\gamma^g) = m_z$. Furthermore, with the aid of the selected AI vector $\mathbf{e}_{\gamma^g}$, the $1 \times N_{\rm g}$ Switch Controller S_2 feeds the CI number $\tilde{\lambda}^g$ into the CI Vector Selector-γ^g. In the γ^g-th CI Vector Selector, the $\tilde{\lambda}^g$-th CI $\bar{\mathbf{e}}_{\tilde{\lambda}^g}^{\gamma^g}$ from the CI vector set $\Delta^{\gamma^g} = \left\{\bar{\mathbf{e}}_1^{\gamma^g}, \cdots, \bar{\mathbf{e}}_{N_{\rm rf}}^{\gamma^g}\right\}$ is used to specify the $\tilde{\lambda}^g$-th channel state $\mathbf{h}_{\tilde{\lambda}^g}^{\gamma^g}$ of the channel states set $\mathbf{H}^{\gamma^g} = \{\mathbf{h}_1^{\gamma^g}, \mathbf{h}_2^{\gamma^g}, \cdots, \mathbf{h}_{N_{\rm rf}}^{\gamma^g}\}$. Finally, the component $\mathbf{C}^g(\gamma^g)$ (i.e., m_z) of the $\mathbf{C}^g$ is modulated by the selected CI vector $\bar{\mathbf{e}}_{\tilde{\lambda}^g}^{\gamma^g}$ on the specified channel state $\mathbf{h}_{\tilde{\lambda}^g}^{\gamma^g}$ to be transmitted. Thus, the quadrature part of the γ^g-th MBM vector $\mathbf{X}_{\gamma^g}^{g}$ on the γ^g-th active TA can be expressed mathematically by

$$\mathbf{X}_{\gamma^g}^{g,\Im} = [\bar{\mathbf{e}}_{\tilde{\lambda}^g}^{\gamma^g} \cdot \mathbf{C}^g(\gamma^g)]^T. \tag{11}$$

Similarly, it is very important to note that the MBM vectors on unactive TAs in the quadrature dimension are set to zero vectors with the size of $1 \times N_{\rm rf}$ dimensions.

Thus, the quadrature part of the MBM vector symbol $\mathbf{Z}^g$ for the output of the g-th block of Bits-Modulator can be expressed as

$$\begin{aligned}\mathbf{Z}^{g,\Im} &= [\mathbf{X}_1^{g,\Im}; \cdots; \mathbf{X}_{N_g}^{g,\Im}] \\ &= [\mathbf{0}_1, \mathbf{0}_2, \cdots, \mathbf{0}_{\gamma^g-1}, \mathbf{X}_{\gamma^g}^{g,\Im}, \mathbf{0}_{\gamma^g+1}, \cdots, \mathbf{0}_{N_g}]\end{aligned} \tag{12}$$

where all zero vectors are the size of $1 \times N_{\rm rf}$ dimensions.

Resultly, by adding the in-phase vector symbol $\mathbf{Z}^{g,\Re}$ in (10) and the quadrature vector symbol $\mathbf{Z}^{g,\Im}$ in (12), the g-th MBM vector symbol $\mathbf{Z}^g$ can be obtained, as is expressed by (13), as shown at the bottom of the next page.

Based on the above design principle in Fig. 2, G blocks of bit sequences: $B_1, B_2, \cdots, B_G$ are modulated into G MBM vector symbols: $\mathbf{Z}^1, \mathbf{Z}^2, \cdots, \mathbf{Z}^G$. Then, concatenating G number of MBM vectors: $\mathbf{Z}^1, \mathbf{Z}^2, \cdots, \mathbf{Z}^G$, the normalized spatial TMV symbol is obtained to be transmitted over the specified channel states, as shown in the normalized form of (1).

To further explain the above design principle of generating the g-th spatial MBM symbol $\mathbf{Z}^g$, EXAMPLEs are given in TABLE 2. Assumed that the mapped 3D signal CP is $s_{\rm 3D} = (m_x, m_y, m_z)$ and $N_g = 4$. According to (4), (5) and the AI vector set of $\Omega_{\bar{\rm C}}$, it has $\Omega_{\bar{\rm A}} = \{\mathbf{a}_1, \mathbf{a}_2\} = \begin{bmatrix} 1 & 0 \\ 0 & 1 \\ 0 & 0 \\ 0 & 0 \end{bmatrix}$, $\Omega_{\bar{\rm B}} = \{\mathbf{b}_1, \mathbf{b}_2\} = \begin{bmatrix} 0 & 0 \\ 0 & 0 \\ 1 & 0 \\ 0 & 1 \end{bmatrix}$, $\Omega_{\bar{\rm C}} = \begin{bmatrix} 1 & 0 & 0 & 0 \\ 0 & 1 & 0 & 0 \\ 0 & 0 & 1 & 0 \\ 0 & 0 & 0 & 1 \end{bmatrix}$, $\Delta^{\gamma^g} = \left\{\bar{\mathbf{e}}_1^{\gamma^g}, \cdots, \bar{\mathbf{e}}_{N_{\rm rf}}^{\gamma^g}\right\} = \begin{bmatrix} 1 & 0 & 0 & 0 \\ 0 & 1 & 0 & 0 \\ 0 & 0 & 1 & 0 \\ 0 & 0 & 0 & 1 \end{bmatrix}$. Note that, the $\mathbf{0}$ vectors is with $N_{\rm rf} \times 1$ dimensions in TABLE 2.

C. RECEIVER

After that G versions from the same 3D mapped symbol $s_{\rm 3D}$ are transmitted over the specified channel states with G groups of CI information bits, each with two subblocks bits: $I_{\rm rf}^{\Re}$ and $I_{\rm rf}^{\Im}$, i.e., the g-th Bit-Modulator contains $I_{\rm rf}^{g,\Re}$ and $I_{\rm rf}^{g,\Im}$. Without loss of generality, with the aid of the AI and CI bits in the g-th Bit-Modulator, two components m_x, m_y (or one component m_z) of the 3D mapped symbol $s_{\rm 3D}$ in the in-phase (or quadrature) dimension are (is) transmitted over the specified channel states of $\mathbf{h}_{\lambda^g}^{i^g}$, $\mathbf{h}_{\frac{N_{\rm g}}{2}+\tilde{\lambda}^g}^{\ell^g}$ (or $\mathbf{h}_{\tilde{\lambda}^g}^{\gamma^g}$). Hence, by combing with (8), (9), (11) and (13), the expression of the formula for the spatial receive vector symbol with $N_{\rm r}$ receive antennas in (3) can be rewritten as

$$\begin{aligned}\mathbf{Y} = \rho \cdot &(\mathbf{h}_{i^1}^1 + \cdots + \mathbf{h}_{i^g}^g + \cdots + \mathbf{h}_{i^G}^G) \cdot m_x \\ &+ (\mathbf{h}_{\ell^1}^1 + \cdots + \mathbf{h}_{\ell^g}^g + \cdots + \mathbf{h}_{\ell^G}^G) \cdot m_y \\ &+ j(\mathbf{h}_{\gamma^1}^1 + \cdots + \mathbf{h}_{\gamma^g}^g + \cdots + \mathbf{h}_{\gamma^G}^G) \cdot m_z + \mathbf{N},\end{aligned} \tag{14}$$

where $\rho = 1/G$.

TABLE 2. Examples of generating the g-th spatial MBM symbol $\mathbf{Z}^g$ to modulate a 3D signal CP $s_{3\mathrm{D}} = (m_x, m_y, m_z)$ with the AI and CI information bits in the g-th Bits-Modulator.

$\Re$ and $\Im$ CI bits		AI bits	AI vectors	CI vectors	Spatial vectors	Spatial MBM symbols
$I_{\mathrm{rf}}^{g,\Re}$	$I_{\mathrm{rf}}^{g,\Im}$	$I_{\bar{\mathrm{A}}}^{g}, I_{\bar{\mathrm{B}}}^{g}, I_{\bar{\mathrm{C}}}^{g}$	$\mathbf{a}_{i^g}, \mathbf{b}_{\ell^g}, \mathbf{e}_{\gamma^g}$	$\bar{\mathbf{e}}_{\lambda^g}^{i^g}, \bar{\mathbf{e}}_{\lambda^g}^{(\frac{N_g}{2}+\ell^g)}, \bar{\mathbf{e}}_{\lambda^g}^{\gamma^g}$	$(\bar{\mathbf{a}}_{i^g})^T, (\bar{\mathbf{b}}_{\ell^g})^T, (\mathbf{C}_{\gamma^g})^T$	$\mathbf{Z}$
00	00	0, 0, 0 0	$\mathbf{a}_1,\ \mathbf{b}_1, \mathbf{e}_1$	$\bar{\mathbf{e}}_1^1, \bar{\mathbf{e}}_1^3, \bar{\mathbf{e}}_1^1$	$[m_x\ 0\ m_y\ 0],\ [m_z\ 0\ 0\ 0]$	$[\bar{\mathbf{e}}_1^1 \cdot (m_x + jm_z); \mathbf{0}, \bar{\mathbf{e}}_1^3 \cdot m_y; \mathbf{0}]^T$
01	00	0, 0, 0 1	$\mathbf{a}_1,\ \mathbf{b}_1, \mathbf{e}_2$	$\bar{\mathbf{e}}_2^1, \bar{\mathbf{e}}_2^3, \bar{\mathbf{e}}_1^2$	$[m_x\ 0\ m_y\ 0],\ [0\ m_z\ 0\ 0]$	$[\bar{\mathbf{e}}_2^1 \cdot m_x; \bar{\mathbf{e}}_1^2 \cdot jm_z; \bar{\mathbf{e}}_2^3 \cdot m_y; \mathbf{0}]^T$
10	00	0, 0, 1 0	$\mathbf{a}_1,\ \mathbf{b}_1, \mathbf{e}_3$	$\bar{\mathbf{e}}_3^1, \bar{\mathbf{e}}_3^3, \bar{\mathbf{e}}_1^3$	$[m_x\ 0\ m_y\ 0],\ [0\ 0\ m_z\ 0]$	$[\bar{\mathbf{e}}_3^1 \cdot m_x; \mathbf{0}; \bar{\mathbf{e}}_3^3 \cdot m_y + \bar{\mathbf{e}}_1^3 \cdot jm_z; \mathbf{0}]^T$
11	00	0, 0, 1 1	$\mathbf{a}_1,\ \mathbf{b}_1, \mathbf{e}_4$	$\bar{\mathbf{e}}_4^1, \bar{\mathbf{e}}_4^3, \bar{\mathbf{e}}_1^4$	$[m_x\ 0\ m_y\ 0],\ [0\ 0\ 0\ m_z]$	$[\bar{\mathbf{e}}_4^1 \cdot m_x; \mathbf{0}; \bar{\mathbf{e}}_4^3 \cdot m_y; \bar{\mathbf{e}}_1^4 \cdot jm_z]^T$
00	01	0, 1, 0 0	$\mathbf{a}_1,\ \mathbf{b}_2, \mathbf{e}_1$	$\bar{\mathbf{e}}_1^1, \bar{\mathbf{e}}_1^4, \bar{\mathbf{e}}_2^1$	$[m_x\ 0\ 0\ m_y],\ [m_z\ 0\ 0\ 0]$	$[\bar{\mathbf{e}}_1^1 \cdot m_x + \bar{\mathbf{e}}_2^1 \cdot jm_z; \mathbf{0}; \mathbf{0}; \bar{\mathbf{e}}_1^4 \cdot m_y]^T$
01	01	0, 1, 0 1	$\mathbf{a}_1,\ \mathbf{b}_2, \mathbf{e}_2$	$\bar{\mathbf{e}}_2^1, \bar{\mathbf{e}}_2^4, \bar{\mathbf{e}}_2^2$	$[m_x\ 0\ 0\ m_y],\ [0\ m_z\ 0\ 0]$	$[\bar{\mathbf{e}}_2^1 \cdot m_x; \bar{\mathbf{e}}_2^2 \cdot jm_z; \mathbf{0}; \bar{\mathbf{e}}_2^4 \cdot m_y]^T$
10	01	0, 1, 1 0	$\mathbf{a}_1,\ \mathbf{b}_2, \mathbf{e}_3$	$\bar{\mathbf{e}}_3^1, \bar{\mathbf{e}}_3^4, \bar{\mathbf{e}}_2^3$	$[m_x\ 0\ 0\ m_y],\ [0\ 0\ m_z\ 0]$	$[\bar{\mathbf{e}}_3^1 \cdot m_x; \mathbf{0}; \bar{\mathbf{e}}_2^3 \cdot jm_z; \bar{\mathbf{e}}_3^4 \cdot m_y]^T$
11	01	0, 1, 1 1	$\mathbf{a}_1,\ \mathbf{b}_2, \mathbf{e}_4$	$\bar{\mathbf{e}}_4^1, \bar{\mathbf{e}}_4^4, \bar{\mathbf{e}}_2^4$	$[m_x\ 0\ 0\ m_y],\ [0\ 0\ 0\ m_z]$	$[\bar{\mathbf{e}}_4^1 \cdot m_x; \mathbf{0}; \mathbf{0}; \bar{\mathbf{e}}_4^4 \cdot m_y + \bar{\mathbf{e}}_2^4 \cdot jm_z]^T$
00	10	1, 0, 0, 0	$\mathbf{a}_2,\ \mathbf{b}_1, \mathbf{e}_1$	$\bar{\mathbf{e}}_1^2, \bar{\mathbf{e}}_1^3, \bar{\mathbf{e}}_3^1$	$[0\ m_x\ m_y\ 0],\ [m_z\ 0\ 0\ 0]$	$[\bar{\mathbf{e}}_3^1 \cdot jm_z; \bar{\mathbf{e}}_1^2 \cdot m_x; \bar{\mathbf{e}}_1^3 \cdot m_y; \mathbf{0}]^T$
01	10	1, 0, 0 1	$\mathbf{a}_2,\ \mathbf{b}_1, \mathbf{e}_2$	$\bar{\mathbf{e}}_2^2, \bar{\mathbf{e}}_2^3, \bar{\mathbf{e}}_3^2$	$[0\ m_x\ m_y\ 0],\ [0\ m_z\ 0\ 0]$	$[\mathbf{0}; \bar{\mathbf{e}}_2^2 \cdot m_x + \bar{\mathbf{e}}_3^2 \cdot jm_z; \bar{\mathbf{e}}_2^3 \cdot m_y; \mathbf{0}]^T$
10	10	1, 0, 1 0	$\mathbf{a}_2,\ \mathbf{b}_1, \mathbf{e}_3$	$\bar{\mathbf{e}}_3^2, \bar{\mathbf{e}}_3^3, \bar{\mathbf{e}}_3^3$	$[0\ m_x\ m_y\ 0],\ [0\ 0\ m_z\ 0]$	$[\mathbf{0}; \bar{\mathbf{e}}_3^2 \cdot m_x; \bar{\mathbf{e}}_3^3 \cdot (m_y + jm_z); \mathbf{0}]^T$
11	10	1, 0, 1 1	$\mathbf{a}_2,\ \mathbf{b}_1, \mathbf{e}_4$	$\bar{\mathbf{e}}_4^2, \bar{\mathbf{e}}_4^3, \bar{\mathbf{e}}_3^4$	$[0\ m_x\ m_y\ 0],\ [0\ 0\ 0\ m_z]$	$[\mathbf{0}; \bar{\mathbf{e}}_4^2 \cdot m_x; \bar{\mathbf{e}}_4^3 \cdot m_y; \bar{\mathbf{e}}_3^4 \cdot jm_z]^T$
00	11	1, 1, 0 0	$\mathbf{a}_2,\ \mathbf{b}_2, \mathbf{e}_1$	$\bar{\mathbf{e}}_1^2, \bar{\mathbf{e}}_1^4, \bar{\mathbf{e}}_4^1$	$[0\ m_x\ 0\ m_y],\ [m_z\ 0\ 0\ 0]$	$[\bar{\mathbf{e}}_4^1 \cdot jm_z; \bar{\mathbf{e}}_1^2 \cdot m_x; \mathbf{0}; \bar{\mathbf{e}}_1^4 \cdot m_y]^T$
01	11	1, 1, 0 1	$\mathbf{a}_2,\ \mathbf{b}_2, \mathbf{e}_2$	$\bar{\mathbf{e}}_2^2, \bar{\mathbf{e}}_2^4, \bar{\mathbf{e}}_4^2$	$[0\ m_x\ 0\ m_y],\ [0\ m_z\ 0\ 0]$	$[\mathbf{0}; \bar{\mathbf{e}}_2^2 \cdot m_x + \bar{\mathbf{e}}_4^2 \cdot jm_z; \mathbf{0}; \bar{\mathbf{e}}_2^4 \cdot m_y]^T$
10	11	1, 1, 1 0	$\mathbf{a}_2,\ \mathbf{b}_2, \mathbf{e}_3$	$\bar{\mathbf{e}}_3^2, \bar{\mathbf{e}}_3^4, \bar{\mathbf{e}}_4^3$	$[0\ m_x\ 0\ m_y],\ [0\ 0\ m_z\ 0]$	$[\mathbf{0}; \bar{\mathbf{e}}_3^2 \cdot m_x; \mathbf{0}; \bar{\mathbf{e}}_4^3 \cdot jm_z; \bar{\mathbf{e}}_3^4 \cdot m_y]^T$
11	11	1, 1, 1 1	$\mathbf{a}_2,\ \mathbf{b}_2, \mathbf{e}_4$	$\bar{\mathbf{e}}_4^2, \bar{\mathbf{e}}_4^4, \bar{\mathbf{e}}_4^4$	$[0\ m_x\ 0\ m_y],\ [0\ 0\ 0\ m_z]$	$[\mathbf{0}; \bar{\mathbf{e}}_4^2 \cdot m_x; \mathbf{0}; \bar{\mathbf{e}}_4^4 \cdot (m_y + jm_z)]^T$

In order to betterly retrieve the incoming bits sequence B, being composed of $B_{3\mathrm{D}}$ and G number of $B_1, \cdots, B_G$, each of which contains five subblocks of $I_{\mathrm{rf}}^{g,\Re}$, $I_{\mathrm{rf}}^{g,\Im}$, $I_{\bar{\mathrm{A}}}^{g}$, $I_{\bar{\mathrm{B}}}^{g}$, $I_{\bar{\mathrm{C}}}^{g}$, the joint detector with Maximum Likelihood (ML) algorithm is employed and formulated as

$$\left[\hat{B}_1, \cdots, \hat{B}_G, \hat{B}_{3\mathrm{D}}\right] = \arg \min_{B_1,\cdots,B_G,B_{3\mathrm{D}}} \left\|\mathbf{Y} - \mathbf{H} \cdot \bar{\mathbf{Z}}\right\|^2, \quad (15)$$

where $\hat{B}_1, \cdots, \hat{B}_G$ are the estimates of G bits blocks of $B_1, \cdots, B_G$, respectively. $\hat{B}_{3\mathrm{D}}$ is the estimate of the bits block of $B_{3\mathrm{D}}$.

III. PERFORMANCE ANALYSIS

In this section, the SEs and the squared MEDs between the TMVs are analyzed to verify the advantage of the TD-QIM-MBM as compared with these classic MBM with IM systems (e.g., SM-MSM, QSM-MBM, GSM-MBM) at the same SE. Moreover, the average bit error probability (BEP) is also derived.

A. COMPARISONS OF THE SPECTRAL EFFICIENCY AND DETECTION COMPLEXITY

Firstly, the SE is analyzed under the same number of both N_{t} and n_{rf} CI bits. According to the design of 2 in each group of Bits-Modulator, the SE of the proposed TD-QIM-MBM can be expressed as

$$\begin{aligned}\eta &= B_1 + \cdots + B_G + B_{3\mathrm{D}} \\ &= \left(2 \cdot n_{\mathrm{rf}} + 2 \cdot \log_2 \frac{N_g}{2} + \log_2 N_g\right) \cdot G + \log_2 M, \quad (16)\end{aligned}$$

where M is the modulation order of the 3D signal constellation. To outstand the advantage of the SE for the proposed TD-QIM-MBM, the comparisons of the SEs for various schemes with employing one signal CP are provided in TABLE 3, where $G = 2$, $M = 8$. Note that, the SEs of SM-MBM, QSM-MBM and QCM-II are respectively $\log_2 N_{\mathrm{t}} + n_{\mathrm{rf}} + \log_2 M$, $2 \cdot \log_2 N_{\mathrm{t}} + 2n_{\mathrm{rf}} + \log_2 M$, $2 \cdot \log_2 N_{\mathrm{t}} + 2n_{\mathrm{rf}} + \log_2 M$. Obviously, it can be seen that, when $N_{\mathrm{t}} = 8$, the TD-QIM-MBM achieves 11, 6, 6 bits over the SM-MBM, QCM-III and QSM-MBM in terms of the SE at the same

$$\begin{aligned}\mathbf{Z}^g &= [\mathbf{X}_1^g, \cdots, \mathbf{X}_{N_g}^g] \\ &= \mathbf{Z}^{g,\Re} + j\mathbf{Z}^{g,\Im} \\ &= \begin{cases} [\mathbf{0}_1, \cdots, \mathbf{X}_{i^g}^{g,\Re} + j\mathbf{X}_{\gamma^g}^{g,\Im}, \mathbf{0}_{i^g+1}, \cdots, \mathbf{0}_{(\frac{N_g}{2}+\ell^g)-1}, \mathbf{X}_{(\frac{N_g}{2}+\ell^g)}^{g,\Re}, \mathbf{0}_{(\frac{N_g}{2}+\ell^g)+1}, \cdots, \mathbf{0}_{N_g}], & i^g = \gamma^g, \frac{N_g}{2} + \ell^g \neq \gamma^g \\ [\mathbf{0}_1, \cdots, \mathbf{X}_{i^g}^{g,\Re}, \mathbf{0}_{i^g+1}, \cdots, \mathbf{0}_{(\frac{N_g}{2}+\ell^g)-1}, \mathbf{X}_{(\frac{N_g}{2}+\ell^g)}^{g,\Re} + j\mathbf{X}_{\gamma^g}^{g,\Im}, \mathbf{0}_{(\frac{N_g}{2}+\ell^g)+1}, \cdots, \mathbf{0}_{N_g}], & i^g \neq \gamma^g, \frac{N_g}{2} + \ell^g = \gamma^g \\ [\mathbf{0}_1, \cdots, \mathbf{X}_{i^g}^{g,\Re}, \mathbf{0}_{i^g+1}, \cdots, \mathbf{0}_{\gamma^g-1}, j\mathbf{X}_{\gamma^g}^{g,\Im}, \mathbf{0}_{\gamma^g+1}, \cdots, \mathbf{X}_{(\frac{N_g}{2}+\ell^g)}^{g,\Re}, \mathbf{0}_{(\frac{N_g}{2}+\ell^g)+1}, \cdots, \mathbf{0}_{N_g}], & i^g \neq \gamma^g, \frac{N_g}{2} + \ell^g \neq \gamma^g \end{cases} \end{aligned} \quad (13)$$

TABLE 3. The SEs for various schemes.

Various Schemes	Spectral Efficiencies [bits/s/Hz]	
	$N_t = 8, n_{rf} = 2$	$N_t = 16, n_{rf} = 2$
TD-QIM-MBM	19	25
QCM-III	13	15
QSM-MBM	13	15
SM-MBM	8	9

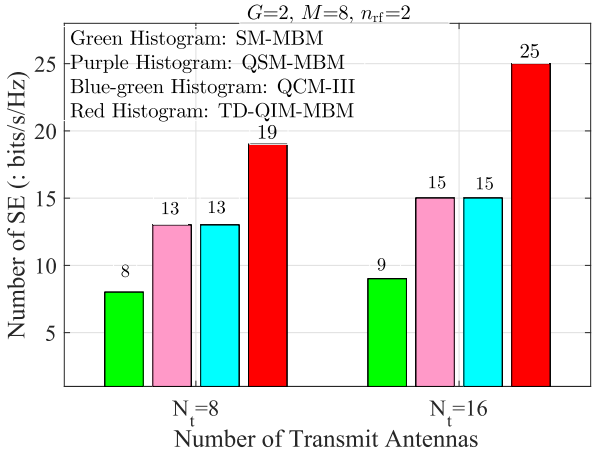

FIGURE 3. The comparisons of SEs between the TD-QIM-MBM with $G = 2$ and the SM-MBM, QCM-III and QSM-MBM schemes at the different TAs, $M = 8$ and $n_{rf} = 2$.

number of TAs, n_{rf}, modulator order M. In order to observe the comparisons of SEs more intuitively, Fig. 3 is provided for the different TAs ($N_t \in \{8,\ 16\}$) with $G = 2,\ M = 8$ and $n_{rf} = 2$. It can be observed that the TD-QIM-MBM has the advantage of the SEs.

Secondly, the detection complexity for the TD-QIM-MBM is introduced and compared with other schemes such as the QSM-MBM and GSM-MBM. Here, using the real multiplication to measure the detection complexity at the receiver. According to the spatial receive vector symbol in Eq. (14) and the Eq. (15), the real multiplications (γ) for the TD-QIM-MBM and various schemes are respectively given by

- SM-MBM: $\gamma_{SM-MBM} = 8 \times N_r \times 2^{\eta}$
- QSM-MBM: $\gamma_{QSM-MBM} = 8 \times N_r \times 2^{\eta}$
- QCM-III: $\gamma_{QCM-II} = 8 \times N_r \times 2^{\eta}$
- GSM-MBM: $\gamma_{GSM-MBM} = (n_a + 1) \times 4N_r \times 2^{\eta}$
- TD-QIM-MBM: $\gamma_{TD-QIM} = (\frac{3}{2}G + 1) \times 4N_r \times 2^{\eta}$.

where n_a is the number of active TAs. Based on the above analysis, when $G > 1$, the real multiplication of the TD-QIM-MBM is inferior to that of the QSM-MBM, QSM-MBM and QCM-III schemes. In addition, according to the parameters of both n_a and G, the real multiplications for the TD-QIM-MBM and GSM-MBM schemes can be calculated. When $n_a = 3$ and $G = 2$, the real multiplication of the TD-QIM-MBM is the same as that of the GSM-MBM. Moreover, under the same complexity of real multiplication, the TD-QIM-MBM has better BER performance than the GSM-MBM, as shown in Fig. 7.

B. ANALYSIS OF THE SQUARED MED BETWEEN THE TMVs

In order to outstand the advantage of the proposed TD-QIM-MBM, the normalized squared MEDs between the TMVs need to be analyzed for different SEs, which can be expressed as

$$d^2_{\min,\bar{\mathbf{Z}}} = \min_{\bar{\mathbf{Z}} \neq \tilde{\bar{\mathbf{Z}}}} \left\| \bar{\mathbf{Z}} - \tilde{\bar{\mathbf{Z}}} \right\|^2. \tag{17}$$

Furthermore, according to several equations of (6), (8), (9), (10), (11) and (12), once there is a misjudgment in the antenna or channel index in one of the G spatial MBM vectors, the squared MEDs can be calculated by

$$\begin{aligned} & d^2_{\min,\bar{\mathbf{Z}}} \\ & = \min_{\bar{\mathbf{Z}} \neq \tilde{\bar{\mathbf{Z}}}} \left\| \bar{\mathbf{Z}} - \tilde{\bar{\mathbf{Z}}} \right\|^2 \\ & = \min \left\{ \frac{2\,|m_x|}{G \cdot E_{av}}, \frac{2\,|m_y|}{G \cdot E_{av}}, \frac{2\,|m_z|}{G \cdot E_{av}} \right\} \\ & = \frac{2}{G \cdot E_{av}}, \end{aligned} \tag{18}$$

where E_{av} is the average energy per 3D signal CP, and noting that $\min\{\,|m_x|\,, |m_y|\,, |m_z|\,\} = 1$. For instance, 16-3DCII CPs: $\{(\pm1, \pm1, \pm2)\,, (\pm1, \pm2, \pm1)\}$, 32-3DCII CPs: $\{(\pm1, \pm1, \pm2), (\pm1, \pm2, \pm1), (\pm2, \pm1, \pm1), (\pm3, \pm1, \pm2)\}$, it can be seen that it has $\min\{|m_x|\} = 1$, or $\min\{|m_y|\} = 1$, or $\min\{|m_z|\} = 1$.

And the results at different SEs for the squared MEDs are listed in TABLE 4. It can be seen from TABLE 4 that the TD-QIM-MBM has the significant advantage of the squared MEDs between two TMVs as compared with the QCM-III, and slight disadvantage as compared with the GSM-MBM. However, the proposed TD-QIM-MBM achieves the transmit diversity but the GSM-MBM has not. Hence, in the terms of the BER performance, the TD-QIM-MBM outperforms the GSM-MBM, which will be verified in the Section IV.

TABLE 4. Comparisons of the squared MED between the TMVs.

$N_t = 8, n_{rf} = 2$	19 bis/s/Hz	20 bis/s/Hz	21 bis/s/Hz
TD-QIM-MBM	2/6	2/12	2/16
GSM-MBM	2/7	2/9	2/11
QCM-III	2/330	2/682	2/1322
$N_t = 8, n_{rf} = 3$	23 bis/s/Hz	24 bis/s/Hz	25 bis/s/Hz
TD-QIM-MBM	2/6	2/12	2/16
GSM-MBM	2/9	2/11	2/13

C. ANALYSIS OF THE BIT ERROR PROBABILITY

In this subsection, the upper bound of the average BEP is analyzed in what follows.

At the receiver, after that the spatial TMV symbol $\bar{\mathbf{Z}}$ is transmitted over the specified fading channels with the additive white Gaussian noise matrix, the detected spatial TMV symbol $\bar{\mathbf{Z}}$ is denoted by $\tilde{\bar{\mathbf{Z}}}$. Based on (3) and Eq. (15), it is shown that the ML detective algorithm is employed for

the TD-QIM-MBM system. Given the channel matrix $\mathbf{H}$, the conditional pairwise error probability (PEP) can be obtained by

$$\begin{aligned} &P(\bar{\mathbf{Z}} \to \tilde{\bar{\mathbf{Z}}}|\mathbf{H}) \\ &= P(\left\|\mathbf{Y} - \mathbf{H}\bar{\mathbf{Z}}\right\|_{\mathrm{F}}^2 > \left\|\mathbf{Y} - \mathbf{H}\tilde{\bar{\mathbf{Z}}}\right\|_{\mathrm{F}}^2 |\mathbf{H}) \\ &= P(U > \left\|\mathbf{H}(\bar{\mathbf{Z}} - \tilde{\bar{\mathbf{Z}}})\right\|_{\mathrm{F}}^2), \end{aligned} \tag{19}$$

where $U = \mathrm{Tr}\left\{\mathbf{n} \cdot [\mathbf{H}(\bar{\mathbf{Z}} - \tilde{\bar{\mathbf{Z}}})]^H + [\mathbf{H}(\bar{\mathbf{Z}} - \tilde{\bar{\mathbf{X}}})] \cdot \mathbf{n}^H\right\}$, $\mathrm{Tr}\{\cdot\}$ denotes the operation of the trace of one matrix. Furthermore, since the parameter U is of chi-squared distribution with $2N_r$ degrees of freedom with zero mean Gaussian random variable with variance $2\sigma^2 \left\|\mathbf{H}(\tilde{\bar{\mathbf{Z}}} - \bar{\mathbf{Z}})\right\|_F^2$, thus the conditional PEP can be given by

$$\begin{aligned} P\left(\bar{\mathbf{Z}} \to \tilde{\bar{\mathbf{Z}}}\right)\Big|\mathbf{H} &= Q\left(\sqrt{\frac{\left\|\mathbf{H}(\mathbf{Z} - \tilde{\bar{\mathbf{Z}}})\right\|_F^2}{2\sigma^2}}\right) \\ &= Q\left(\sqrt{\frac{\mathrm{Tr}[\mathbf{H} \cdot \Delta \cdot \mathbf{H}^H]}{2\sigma^2}}\right), \end{aligned} \tag{20}$$

where $Q(\cdot)$ is the Q function denoted by $Q(x) = \frac{1}{\pi}\int_0^{\frac{\pi}{2}} \exp\left(\frac{-x^2}{2\sin^2\theta}\right)d\theta$. $\Delta = \left(\bar{\mathbf{Z}} - \tilde{\bar{\mathbf{Z}}}\right) \cdot \left(\bar{\mathbf{Z}} - \tilde{\bar{\mathbf{Z}}}\right)^H$, $\{\cdot\}^H$ denotes the operation of the transposition.

Then, the expectation on (20) with the channel matrix $\mathbf{H}$ is taken. After calculating it, the closed form expression of the unconditional PEP [26] can be obtained as

$$\begin{aligned} &P\left(\bar{\mathbf{Z}} \to \tilde{\bar{\mathbf{Z}}}\right) \\ &= E_{\mathbf{H}}\left\{P\left(\bar{\mathbf{Z}} \to \tilde{\bar{\mathbf{Z}}}\right)\Big|\mathbf{H}\right\} \\ &= \frac{1}{\pi}\int_0^{\frac{\pi}{2}} \exp\left(\frac{-E_{\mathbf{H}}\left\{\mathrm{Tr}[\mathbf{H} \cdot \Delta \cdot \mathbf{H}^H]\right\}}{4\sigma^2\sin^2\theta}\right)d\theta \\ &\geq \frac{1}{\pi}\int_0^{\frac{\pi}{2}} \exp\left\{\frac{-d^2_{\min,\bar{\mathbf{Z}}}}{4\sigma^2\sin^2\theta} \cdot \left\{\sum_{\beta=1}^{\tau \cdot G}\sum_{\alpha=1}^{N_{\mathrm{r}}}\left|h_{\lambda,\alpha}^{\kappa_\beta}\right|^2\right\}\right\}d\theta \\ &= \frac{1}{\pi}\int_0^{\frac{\pi}{2}} \prod_{\beta=1}^{\tau \cdot G}\prod_{\alpha=1}^{N_{\mathrm{r}}} \exp\left\{\frac{-d^2_{\min,\bar{\mathbf{Z}}} \cdot \left|h_{\lambda,\alpha}^{\kappa_\beta}\right|^2}{4\sigma^2\sin^2\theta}\right\}d\theta, \end{aligned} \tag{21}$$

where $d^2_{\min,\bar{\mathbf{Z}}}$ is obtained by (18), $\tau \in \{2, 3\}$ is the total number of the activated TAs. $h_{\lambda,\alpha}^{\kappa_\beta}$ is the λ-th channel state between the N_{rf} channel states at the κ_β-th TA and the α-th receiver antenna.

Then, using the moment generating function (MGF) technique [26], the average PEP of (21) can be given by

$$P\left(\bar{\mathbf{Z}} \to \tilde{\bar{\mathbf{Z}}}\right) = \frac{1}{\pi}\int_0^{\frac{\pi}{2}}\left[\frac{\sin^2\theta}{\sin^2\theta + \frac{d^2_{\min,\bar{\mathbf{Z}}}}{4\sigma^2}}\right]^{\tau \cdot G \times N_{\mathrm{r}}} d\theta \tag{22}$$

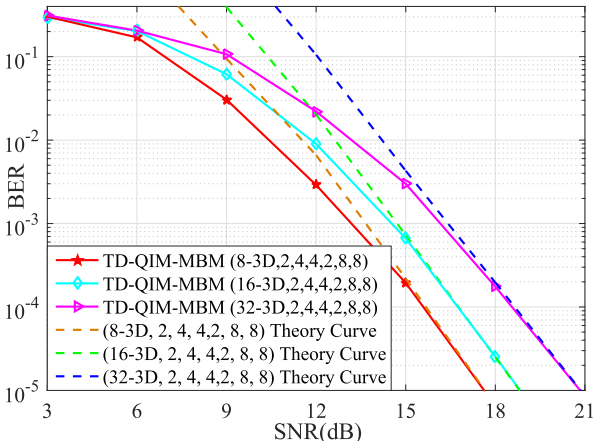

FIGURE 4. Theoretical and simulation results for the TD-QIM-MBM with three cases of (8-3D, 2, 4, 4, 2, 8, 8), (16-3D, 2, 4, 4, 2, 8, 8), (32-3D, 2, 4, 4, 2, 8, 8), and $n_{\mathrm{rf}} = 2$ RF mirrors.

Therefore, the diversity order of the TD-QIM-MBM is $\tau \cdot G \times N_{\mathrm{r}}$, where transmit diversity order is $\tau \cdot G$.

Based on the above analysis and calculation operation, the average BEP may be given by

$$P_b \leq \frac{1}{2^B}\sum_{\bar{\mathbf{Z}}}\sum_{\bar{\mathbf{Z}} \neq \tilde{\bar{\mathbf{Z}}}} \frac{P\left(\bar{\mathbf{Z}} \to \tilde{\bar{\mathbf{Z}}}\right) \cdot e\left(\bar{\mathbf{Z}}, \tilde{\bar{\mathbf{Z}}}\right)}{B}, \tag{23}$$

where $e(\bar{\mathbf{Z}} \to \tilde{\bar{\mathbf{Z}}})$ denotes the total number of erroneous bits when $\bar{\mathbf{Z}}$ is not equal to $\tilde{\bar{\mathbf{Z}}}$.

IV. NUMERICAL RESULTS AND DISCUSSIONS

In this section, the BER vs SNR curves for the TD-QIM-MBM, the SM/QSM-MBM, the GSM-MBM and QCM-III are depicted in the following simulation results. Then, the BER comparisons are performed and discussed. In our simulation results with MATLAB, at the receiver the ML detector is employed and the channel states information is perfectly known, and $(N_{\mathrm{t}}, N_{\mathrm{r}}) = (8, 8)$, $n_{\mathrm{rf}} \in \{2, 3\}$. For the intuitively expression of the parameters of the proposed TD-QIM-MBM and GSM-MBM, QCM-III, QSM-MBM and SM-MBM, the $(L,\ G,\ N_1,\ \cdots,\ N_G,\ n_{\mathrm{rf}},\ N_{\mathrm{t}}, N_{\mathrm{r}})$, $(L_1, L_2, L_3, n_{\mathrm{rf}}, N_{\mathrm{t}}, N_{\mathrm{r}})$, $(L_4, n_{\mathrm{rf}}, N_{\mathrm{t}}, N_{\mathrm{r}})$, $(L_5, n_{\mathrm{rf}}, N_{\mathrm{t}}, N_{\mathrm{r}})$ and $(L_6,\ n_{\mathrm{rf}},\ N_{\mathrm{t}},\ N_{\mathrm{r}})$ are defined for the TD-QIM-MBM, GSM-MBM, QCM-III, QSM-MBM and SM-MBM systems, respectively, where $L_1,\ L_2,\ L_3,\ L_4,\ L_5,\ L_6$ denote the size of modulation orders in QAM signal constellation.

In Fig. 4 with different SEs of 19, 20, 21 bits/s/Hz, the BER performances of the TD-QIM-MBM are presented and made comparison with their theoretical results that are obtained from the average BEP in (23) for three cases of (8-3D, 2, 4, 4, 2, 8, 8), (16-3D, 2, 4, 4, 2, 8, 8), (32-3D, 2, 4, 4, 2, 8, 8). Obviously, it can be observed that, the simulation results of the TD-QIM-MBM match close well with their theoretical results in the high SNR region. Thus, the effectiveness of the TD-QIM-MBM has been verified.

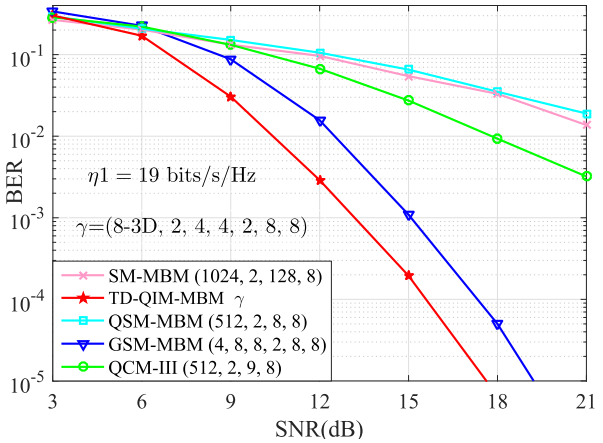

FIGURE 5. BER performance comparisons between the TD-QIM-MBM with (8-3D, 2, 4, 4, 2, 8, 8), the GSM-MBM with (4, 8, 8, 2, 8, 8), the QCM-III with (512, 2, 9, 8), the QSM-MBM with (512, 2, 8, 8) and the SM-MBM with (1024, 2, 128, 8), $n_{rf} = 2$ RF mirrors.

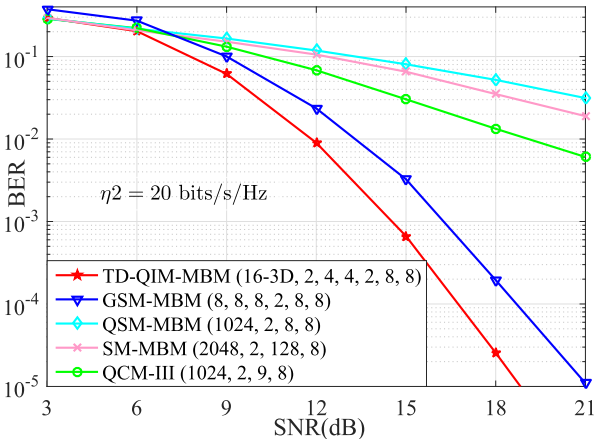

FIGURE 6. BER performance comparisons between the TD-QIM-MBM with (16-3D, 2, 4, 4, 2, 8, 8), the GSM-MBM with (8, 8, 8, 2, 8, 8), the QCM-III with (1024, 2, 9, 8), the QSM-MBM with (1024, 2, 8, 8) and the SM-MBM with (2048, 2, 128, 8) $n_{rf} = 2$ RF mirrors.

Fig. 5 depicts the simulation curves for the TD-QIM-MBM with (8-3D, 2, 4, 4, 2, 8, 8), the GSM-MBM with (4, 8, 8, 2, 8, 8) and the QCM-III with (512, 2, 9, 8). In Fig. 5, at the SE of 19 bits/s/Hz, according to the squared MED analyzed in TABLE 4, the TD-QIM-MBM has the significant advantage as compared with the QCM-III with 512-ary QAM constellation in terms of the squared MED. Hence, in terms of the BER comparison, the TD-QIM-MBM achieves the significant BER performance as compared with the QCM-III. In addition, although the squared MED for the GSM-MBM has slight bigger than the proposed TD-QIM-MBM, the TD-QIM-MBM has better BER performance than the GSM-MBM due to achieving transmit diversity. For instance, 1.5 dB SNR gains over the GSM-MBM are achieved at the BER value of 10^{-3}. Meanwhile, compared with the SM-MBM and QSM-MBM systems, the TD-QIM-MBM achieves significantly BER performance over them.

Fig. 6 depicts the simulation curves of the TD-QIM-MBM with (16-3D, 2, 4, 4, 2, 8, 8) and the GSM-MBM with (8, 8, 8, 2, 8, 8) and the QCM-III with (1024, 2, 9, 8) at 20 bits/s/Hz. Similarly, in terms of the BER performance comparison between the TD-QIM-MBM, the GSM-MBM and the QCM-III, it can be seen from Fig. 6 that the TD-QIM-MBM significantly outperform the GSM-MBM and the QCM-III. It can be also observed that, compared with the GSM-MBM and the QCM-III, more 1.5 dB SNR gains are achieved for the the TD-QIM-MBM at the BER value of 10^{-2}. Meanwhile, the TD-QIM-MBM achieves significantly BER performance in comparisons with the SM-MBM and QSM-MBM systems.

Additionally, to further outstand the advantage of the BER performance for the TD-QIM-MBM, we present the BER versus SNR curves of the TD-QIM-MBM with the consideration of $n_{rf} = 3$ at the SEs of 23, 24 bits/s/Hz in Fig. 7. With the design of $n_{rf} = 3$, the proposed TD-QIM-MBM improve the squared MED. At the SE of 23 bits/s/Hz,

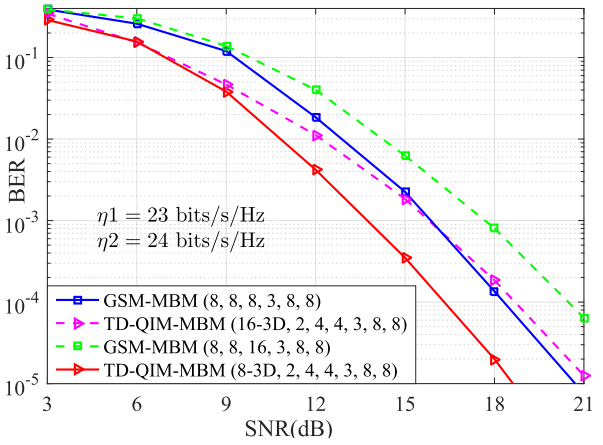

FIGURE 7. BER performance comparisons between the TD-QIM-MBM with both (8-3D, 2, 4, 4, 3, 8, 8) and (16-3D, 2, 4, 4, 2, 8, 8) and the GSM-MBM with both (8, 8, 8, 3, 8, 8) and (8, 8, 16, 3, 8, 8), and $n_{rf} = 3$ RF mirrors.

Fig. 7 shows that approximately 2.3 dB SNR gains over the GSM-MBM with (8, 8, 8, 3, 8, 8) are achieved for the TD-QIM-MBM with (8-3D, 2, 4, 4, 3, 8, 8) at the BER value of 10^{-2}. At the SE of 4 bits/s/Hz, the TD-QIM-MBM with (16-3D, 2, 4, 4, 3, 8, 8) also significantly outperforms the GSM-MBM with the GSM-MBM with (8, 8, 16, 3, 8, 8) in term of the BER values comparison, about 2 dB SNR gains are achieved at the BER value of 10^{-2}.

V. CONCLUSION

In this paper, a new design of TD-QIM-MBM, which develops the transmit diversity and the CI additional information, is proposed to enhance the reliability of wireless communications. On the one hand, the transmit diversity is obtained by designing multiple groups of Bits-Modulator to modulate one and the same mapped 3D signal CP. On the other hand, in each module of Bits-Modulator, the SE is further improved

by designing three specified SVs with three parts of AI bits to modulate three components of the same mapped 3D signal CP on the specified active TAs, resulting in the in-phase and quadrature SV symbols. Then, with the in-phase and quadrature CI bits, the in-phase and quadrature SV symbol are transmitted over the specified channel states. Finally, the performance analysis, including the squared MED and the average BEP, is analyzed. In the numerical results, the TD-QIM-MBM is demonstrated that it outperforms the traditional design systems such as GSM-MBM and QCM-III in terms of the BER performance for enhancing the reliability of MBM-based wireless communications. Next, considering the large MIMO antennas, the DT-QIM-MBM system for multi-user scenarios is investigated.

REFERENCES

[1] J. Wang, S. Jia, and J. Song, "Generalised spatial modulation system with multiple active transmit antennas and low complexity detection scheme," *IEEE Trans. Wireless Commun.*, vol. 11, no. 4, pp. 1605–1615, Apr. 2012.

[2] R. Mesleh, S. S. Ikki, and H. M. Aggoune, "Quadrature spatial modulation," *IEEE Trans. Veh. Technol.*, vol. 64, no. 6, pp. 2738–2742, Jun. 2015.

[3] F. R. Castillo-Soria, J. Cortez, C. A. Gutiérrez, M. Luna-Rivera, and A. Garcia-Barrientos, "Extended quadrature spatial modulation for MIMO wireless communications," *Phys. Commun.*, vol. 32, pp. 88–95, Feb. 2019.

[4] F. R. Castillo-Soria, J. Cortez-González, R. Ramirez-Gutierrez, F. M. Maciel-Barboza, and L. Soriano-Equigua, "Generalized quadrature spatial modulation scheme using antenna grouping," *ETRI J.*, vol. 39, no. 5, pp. 707–717, Oct. 2017.

[5] F. Huang and D. Li, "Extended space index modulation," *IEEE Wireless Commun. Lett.*, vol. 11, no. 6, pp. 1171–1175, Jun. 2022.

[6] A. M. Abu-Hudrouss, M.-T. O. E. Astal, A. H. Al Habbash, and S. Aïssa, "Signed quadrature spatial modulation for MIMO systems," *IEEE Trans. Veh. Technol.*, vol. 69, no. 3, pp. 2740–2746, Mar. 2020.

[7] F. Huang, X. Liu, Z. Zhou, J. Luo, and J. Wang, "Quadrature index modulation with three-dimension constellation," *IEEE Access*, vol. 7, pp. 182335–182347, 2019.

[8] Y. Zhan and F. Huang, "Generalized spatial modulation with multi-index modulation," *IEEE Commun. Lett.*, vol. 24, no. 3, pp. 585–588, Mar. 2020.

[9] F. Huang and Y. Zhan, "Design of spatial constellation for spatial modulation," *IEEE Wireless Commun. Lett.*, vol. 9, no. 7, pp. 1097–1100, Jul. 2020.

[10] F. Huang and D. Li, "Spatial modulation with joint permutation, group and antenna indexes," *IEEE Wireless Commun. Lett.*, vol. 12, no. 4, pp. 753–757, Apr. 2023.

[11] G. Kaddoum, Y. Nijsure, and H. Tran, "Generalized code index modulation technique for high-data-rate communication systems," *IEEE Trans. Veh. Technol.*, vol. 65, no. 9, pp. 7000–7009, Sep. 2016.

[12] G. Zhang, X.-Q. Jiang, H. Hai, M. Wen, P. Shang, and S. Wei, "Joint code index modulation aided enhanced spatial modulation for high-rate MIMO systems," *IEEE Trans. Green Commun. Netw.*, vol. 7, no. 3, pp. 1383–1393, Sep. 2023.

[13] A. K. Khandani, "Media-based modulation: Converting static Rayleigh fading to AWGN," in *Proc. IEEE Int. Symp. Inf. Theory*, Honolulu, HI, USA, Jun. 2014, pp. 1549–1553.

[14] J. Jeganathan, A. Ghrayeb, L. Szczecinski, and A. Ceron, "Space shift keying modulation for MIMO channels," *IEEE Trans. Wireless Commun.*, vol. 8, no. 7, pp. 3692–3703, Jul. 2009.

[15] B. Shamasundar, K. M. Krishnan, T. L. Narasimhan, and A. Chockalingam, "MAP-index coded media-based modulation," *IEEE Commun. Lett.*, vol. 22, no. 12, pp. 2455–2458, Dec. 2018.

[16] E. Aydin, "A new hexagonal quadrature amplitude modulation aided media-based modulation," *Int. J. Commun. Syst.*, vol. 34, no. 17, pp. 1–12, Nov. 2021.

[17] A. J. Bamisaye and T. Quazi, "Quadrature spatial modulation-aided single-input multiple-output-media-based modulation," *Int. J. Commun. Syst.*, vol. 34, no. 11, pp. 1–16, Jul. 2021.

[18] Y. Naresh and A. Chockalingam, "On media-based modulation using RF mirrors," *IEEE Trans. Veh. Technol.*, vol. 66, no. 6, pp. 4967–4983, Jun. 2017.

[19] N. Pillay and H. Xu, "Quadrature spatial media-based modulation with RF mirrors," *IET Commun.*, vol. 11, no. 16, pp. 2440–2448, Nov. 2017.

[20] I. Yildirim, E. Basar, and I. Altunbas, "Quadrature channel modulation," *IEEE Wireless Commun. Lett.*, vol. 6, no. 6, pp. 790–793, Dec. 2017.

[21] E. Basar and I. Altunbas, "Space-time channel modulation," *IEEE Trans. Veh. Technol.*, vol. 66, no. 8, pp. 7609–7614, Aug. 2017.

[22] Z. Yigit and E. Basar, "Space-time media-based modulation," *IEEE Trans. Signal Process.*, vol. 67, no. 9, pp. 2389–2398, May 2019.

[23] S. M. Alamouti, "A simple transmit diversity technique for wireless communications," IEEE J. Sel. Areas Commun., vol. 16, no. 8, p. 145C1458, Oct. 1998.

[24] C. Li, L. Wang, and G. Nie, "Quadrature spatial modulation aided media-based modulation," *IEEE Commun. Lett.*, vol. 26, no. 8, pp. 1928–1932, Aug. 2022.

[25] S. Oladoyinbo, N. Pillay, and H. Xu, "Media-based single-symbol generalized spatial modulation," *Int. J. Commun. Syst.*, vol. 32, no. 6, pp. 1–13, Apr. 2019.

[26] M. K. Simon and M. Alouini, *Digital Communication Over Fading Channels*, 2nd ed. Hoboken, NJ, USA: Wiley, 2005.

XIAOPIN WANG received the B.E. degree in telecommunications engineering from Shandong University of Science and Technology, China, in 2004, and the M.E. degree in electronics and communication technology from Jinan University, China, in 2010. She is currently a Visiting Scholar with the South China University of Technology, China, in 2023. Her current research interests include wireless communication and artificial intelligence application.

SHUQING LIN received the B.S. and M.E. degrees in computer electronics and engineering from South China Normal University, China, in 2002 and 2006, respectively. His current research interests include computer algorithm design and artificial intelligence application.

FUCHUN HUANG received the B.E. degree in electronics information engineering from Henan Polytechnic University, China, in 2008, the M.E. degree from Jiangsu University, in 2012, and the Ph.D. degree in telecommunication and information system from Sun Yat-sen University, China, in 2020. His current research interests include index modulation, spatial constellation design, antenna selection algorithms, and OFDM.